

# The QCD phase diagram for small densities from imaginary chemical potential

Philippe de Forcrand<sup>a,b</sup> and Owe Philipsen<sup>c</sup>

<sup>a</sup> *Institut für Theoretische Physik, ETH Zürich, CH-8093 Zürich, Switzerland*

<sup>b</sup> *Theory Division, CERN, CH-1211 Geneva 23, Switzerland*

<sup>c</sup> *Center for Theoretical Physics, Massachusetts Institute of Technology,  
Cambridge, MA 02139-4307, USA*

## Abstract

We present results on the QCD phase diagram for  $\mu_B \leq \pi T$ . Our simulations are performed with an imaginary chemical potential  $\mu = i\mu_I$  for which the fermion determinant is positive. On an  $8^3 \times 4$  lattice with 2 flavors of staggered quarks, we map out the phase diagram and identify the (pseudo-)critical temperature  $T_c(\mu_I)$ . For  $\mu_I/T \leq \pi/3$ , this is an analytic function, whose Taylor expansion is found to converge rapidly, with truncation errors far smaller than statistical ones. The truncated series may then be continued to real  $\mu$ , yielding the corresponding phase diagram for  $\mu_B \lesssim 500$  MeV. This approach provides control over systematics and avoids reweighting. We compare it with other recent work.

# 1 Introduction

A prime goal of heavy ion collision experiments at SPS, LHC (CERN) and RHIC (Brookhaven) is to probe the transition<sup>1</sup> from hadronic matter to a quark gluon plasma at high temperatures and small baryon density. Because QCD is strongly interacting, the only first principles method to predict the phase diagram is by means of lattice simulations. On the other hand, at finite densities the fermion determinant is complex, thus prohibiting standard Monte Carlo sampling of the path integral in what is known as the ‘sign problem’. Overviews with references to various studies of this problem may be found in [1].

Recently, a first  $(\mu, T)$  phase diagram for 2+1-flavor QCD has been presented [2] by using a two-dimensional generalization [3] of the Glasgow reweighting method [4]. For such methods cancellations in the reweighting factor occur generically at large volumes and/or chemical potentials, and it remains to be seen how well this approach allows for infinite volume and continuum extrapolations. Another work [5] attempts to improve on this aspect by expanding the product of reweighting factor and observable in powers of  $(\mu/T)$ , and computing the coefficients through second order. The calculation is then equivalent to computing susceptibilities at  $\mu = 0$  [6], which is possible on any volume. The  $\mu/T$ -range of applicability is limited by either the  $\mu/T$ -value of the expected critical point marking the onset of a phase transition, where susceptibilities become non-analytic, or the radius of convergence of the expansion, whichever is lower. However, a priori nothing is known about the convergence of the expansion or the error introduced by its truncation. Moreover, a problem common to all reweighting approaches is that so far it has been impossible to assess the overlap of reweighted ensembles with the original. Hence, the results obtained in [2, 5] rest on as yet uncontrolled approximations.

In this paper we attempt to develop a controllable alternative approach, avoiding reweighting in  $\mu$  altogether. This is achieved by simulating with imaginary chemical potential, where there is no sign problem and hence no need for reweighting. We employ the idea [7] that in this case one may fit the non-perturbative data for an observable by truncated Taylor series in  $\mu/T$ , thus keeping full control over the associated systematic error. In the parameter range where this is possible, and in the absence of non-analyticities, the series may be analytically continued to real values of  $\mu$ . Non-perturbative evidence for the viability of this approach has been given for screening

---

<sup>1</sup>In this paper the term “transition” is used to label a change in dynamics, whether it proceeds by a smooth crossover or by a first or second order phase transition. For the last two, we use explicitly the term “phase transition”.

masses in the deconfined phase [8], which can be simulated successfully for real and imaginary  $\mu$  [9] in the framework of dimensionally reduced QCD [10]. Here we extend this approach to the critical line  $T_c(\mu)$ . This is possible by noting that, while giving the location of singularities in thermodynamic limit, the critical line itself is an analytic function. After continuing it from imaginary to real  $\mu$  for various volumes, a finite volume scaling analysis of its location should also reveal the nature of the transition. Since there is no sign problem, there are no limitations on the volumes that can be simulated either. In particular, it should then be possible to identify the location of the critical endpoint of the phase transition which is expected on general theoretical grounds [11], and for which reweighted numerical results have been presented in [2].

Our method is limited by a maximal imaginary part of the chemical potential,  $\mu_I^c = \pi T/3$ , above which the system tunnels into an unphysical  $Z(3)$  sector. Along the transition line, this corresponds to an accessible range of real  $\mu_B \lesssim 500$  MeV, which well covers densities in heavy ion experiments [12]. We present numerical results for the location of the critical line, and find that the truncation error of the Taylor series is far smaller than statistical errors in the whole accessible range. A finite volume scaling analysis is beyond the scope of our current computational resources and postponed to later work. Nevertheless, our results indicate that the part of the phase diagram relevant for heavy ion collisions can be reliably obtained from simulations of imaginary chemical potentials.

In Sec. 2 we recall some general features of QCD at imaginary chemical potential, which will be useful in the sequel. The analyticity of the critical line is derived in Sec. 3. Numerical results for two flavor QCD with Wilson gauge action and Kogut-Susskind fermions are presented in Sec. 4, while Sec. 5 discusses our approach in comparison with previous ones. In Sec. 6 we draw our conclusions.

## 2 QCD at real and imaginary chemical potential

While this section contains no new results, we would like to discuss some qualitative features in detail as they play an important role for the following. We denote by  $\mu$  the chemical potential for quark number  $Q$ , and by  $\mu_B$  the chemical potential for baryon number  $B = Q/3$ , i.e.  $\mu = \mu_B/3$ . The grand canonical partition function is compactly written as

$$Z(V, \mu, T) = \text{Tr} \left( e^{-(\hat{H} - \mu \hat{Q})/T} \right). \quad (1)$$

An expansion for small chemical potentials proceeds in terms of the dimensionless parameter  $\bar{\mu} = \mu/T$ , and hence our interest is in  $Z(V, \bar{\mu}, T)$ .

The presence of a chemical potential term in the action breaks the separate invariance under Euclidean time reflection and charge conjugation. In particular, a time reflection can be compensated by  $\mu \rightarrow -\mu$  and vice versa, so that

$$Z(\bar{\mu}) = Z(-\bar{\mu}). \quad (2)$$

As a consequence, observables symmetric under time reflection are even functions of  $\bar{\mu}$ .

Let  $\mu_R, \mu_I \in \mathbb{R}$  denote the real and imaginary parts of  $\mu$ :

$$\mu = \mu_R + i\mu_I, \quad (3)$$

and similarly for  $\bar{\mu}$ . The qualitative features of SU(N) QCD at imaginary chemical potential,  $\mu_R = 0$ , were studied a long time ago [13]. With dynamical fermions the  $Z(N)$  symmetry of the pure gauge theory is explicitly broken. However, in the presence of a complex chemical potential, a  $Z(N)$  transformation of the fermion fields is equivalent to a shift in  $\mu_I$ , thus leading to a new symmetry: the partition function is periodic in  $\mu_I$  with period  $2\pi T/N$  [13],

$$Z(\bar{\mu}_R, \bar{\mu}_I) = Z(\bar{\mu}_R, \bar{\mu}_I + 2\pi/N). \quad (4)$$

The different  $Z(N)$  sectors are characterized by the phase  $\varphi$  of the Polyakov loop,

$$\langle P(x) \rangle = |\langle P(x) \rangle| e^{i\varphi}. \quad (5)$$

At high temperatures one may use the perturbative effective potential  $V(\varphi)$  to obtain the qualitative behaviour of the theory. In pure gauge theory  $\langle P(x) \rangle = 0$  for  $T < T_c$  and  $\langle P(x) \rangle \neq 0$  for  $T > T_c$ . In the deconfined phase there are  $N$  degenerate minima at  $\varphi = 2\pi k/N, k = 1, \dots, N$ , separated by potential barriers, and the transition between them is of first order [14]. For  $N_f > 0, \mu = 0$ , explicit  $Z(N)$ -breaking results in an expectation value for the Polyakov loop even in the confinement phase. The expectation value is real,  $\varphi = 0$ , corresponding to the true vacuum of the theory, while the other sectors are metastable [15]. This is true both for  $T > T_c$  and  $T < T_c$ . When a chemical potential is switched on [13, 16, 17], its real part stabilizes this situation by raising the energy of the other  $Z(N)$  vacua, while the imaginary part has the opposite effect of lowering one of them relative to the  $\varphi = 0$  vacuum. Hence, once  $\mu_I$  exceeds some critical value  $\mu_I^c$ , a phase transition to a non-trivial  $Z(N)$  sector occurs. Non-perturbatively the same statement follows from the aforementioned equivalence of certain  $\mu_I$ -shifts and  $Z(N)$  rotations. The combined symmetries Eqs. (2),(4) imply that this transition is periodically repeated for larger values of  $\mu_I$ . Moreover, its exact critical values are dictated to be [13]

$$\bar{\mu}_I^c = \frac{2\pi}{N} \left( k + \frac{1}{2} \right). \quad (6)$$

On the other hand, for purely real  $\mu$  this transition never occurs. This situation is sketched qualitatively for  $SU(3)$  in Fig. 1. The order of the  $Z(3)$  transitions depends

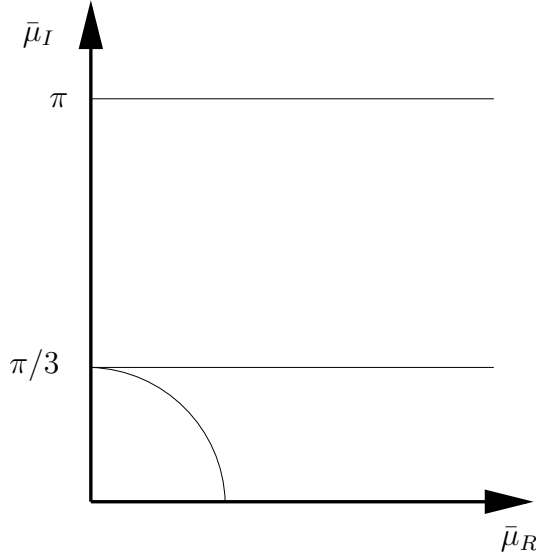


Figure 1: *Location of  $Z(3)$  transitions, Eq. (6). Analytic continuation is limited to the region within the arc.*

on temperature. A perturbative calculation predicts it to be of first order in the deconfined phase, whereas at low temperature a strong coupling analysis suggests it to be a smooth crossover [13]. We shall present numerical results in support of this picture in Sec. 4.

Note that the first of these  $Z(3)$  transitions at  $\bar{\mu}_I^c = \pi/3$  limits the useful information to be obtained from imaginary chemical potentials: Eqs. (2),(4) imply

$$Z(\bar{\mu}_I = \pi/3 + \Delta\bar{\mu}_I) = Z(\bar{\mu}_I = \pi/3 - \Delta\bar{\mu}_I) \quad (7)$$

so that all observables are symmetric about the transition at  $\bar{\mu}_I^c$ . In other words, all expectation values for  $\bar{\mu}_I > \bar{\mu}_I^c$  are simply copies of those for  $\bar{\mu}_I < \bar{\mu}_I^c$ , determined by reflection symmetry and periodicity. Moreover, here we are interested in analytically continuing results obtained on the imaginary axis, and this is only possible for  $|\bar{\mu}| \leq \pi/3$  [8], represented by the arc of circle in Fig. 1. Furthermore, the observable to be continued has to be free of additional singularities in this region. In the next section we will show that this is the case for the critical coupling for deconfinement, and hence the associated temperature  $T_c(\mu)$ . Along the deconfinement transition the latter is in

the range  $T \sim 160 - 170$  MeV, which means that our approach is restricted to baryon chemical potentials  $\mu_B \lesssim 500$  MeV.

### 3 Analyticity of the (pseudo-) critical line

On a  $L^3 \times N_t$  lattice, the rescaled chemical potential takes the form  $\bar{\mu} = N_t a \mu$ , which up to the constant factor  $N_t$  is equivalent to the chemical potential in lattice units. On the lattice one then explores the phase diagram in the  $(\beta, \bar{\mu})$ -plane, which in the continuum limit has to be converted to a  $(T, \mu)$ -diagram.

The location and nature of a phase transition may be determined from the finite volume scaling of susceptibilities of dimensionless operators ( $V = L^3$ ),

$$\chi = V N_t \langle (\mathcal{O} - \langle \mathcal{O} \rangle)^2 \rangle, \quad \mathcal{O} = \frac{1}{V N_t} \sum_{\mathbf{x}, t} \mathcal{O}(x). \quad (8)$$

In practice we shall use as  $\mathcal{O}(x)$  the plaquette, the chiral condensate and the modulus of the Polyakov loop. In a transition region, fluctuations are strong and susceptibilities display a peak,  $\chi_{max} = \chi(\bar{\mu}_c, \beta_c)$ , whose location determines the critical parameters. In a finite volume, the susceptibility is always an analytic function of the parameters of the theory, even in the presence of a phase transition. The latter reveals itself by a divergence of  $\chi_{max}$  in the infinite volume limit, whereas  $\chi_{max}$  stays finite in the case of a crossover. The order of the transition is determined by the rate of divergence: for a first order transition  $\chi_{max} \propto V$ , whereas for a second order phase transition,  $\chi_{max} \propto V^\rho$  with a critical exponent  $\rho = \gamma/d\nu < 1$  [18]. Alternatively, one may consider the finite size scaling of the critical coupling  $\beta_c(V)$  itself, which attains its infinite volume limit as

$$(\beta_c(V) - \beta_c(\infty)) \sim V^{-\sigma}, \quad (9)$$

where  $\sigma = 1$  for a first order phase transition,  $\sigma = 1/d\nu < 1$  for a second order phase transition, and  $\sigma = 0$  for a crossover. (For notation and numerical application to SU(3) pure gauge theory, see e. g. [19] and references therein).

At zero density, the deconfinement transition is signalled by a peak  $\chi_{max} = \chi(0, \beta_c)$ , defining the critical coupling through the equations

$$\left. \frac{\partial \chi}{\partial \beta} \right|_{\beta_c} = 0 \quad \left. \frac{\partial^2 \chi}{\partial \beta^2} \right|_{\beta_c} < 0. \quad (10)$$

When the chemical potential is switched on, this peak extends as a “mountain ridge” into the  $(\beta, \bar{\mu})$ -plane. Starting at  $\beta_c(0)$ , the ridge is defined by maximizing  $\chi$  while

moving into the  $(\beta, \bar{\mu})$ -plane, i.e. by moving along the direction of the gradient  $\nabla\chi(\bar{\mu}, \beta)$  (or the direction with the largest second derivative in the case of vanishing gradient). It has a vanishing first and negative second derivative in the direction perpendicular to the gradient.

For the numerical analysis, however, it is more convenient to consider maxima in the directions of  $\beta$  and  $\bar{\mu}$ , respectively. The two pairs of conditions

$$\left\{ \partial_{\beta}\chi = 0, \partial_{\beta}^2\chi < 0 \right\}, \quad \left\{ \partial_{\bar{\mu}}\chi = 0, \partial_{\bar{\mu}}^2\chi < 0 \right\} \quad (11)$$

then define two separate lines bounding the ridge from below and above, as indicated in Fig. 2 (left), where the ordering of the lines depends on the sign of the gradient. For large enough volumes one expects a positive gradient while increasing  $\mu$  towards a critical point, and the first condition denotes the lower line. When the volume is taken

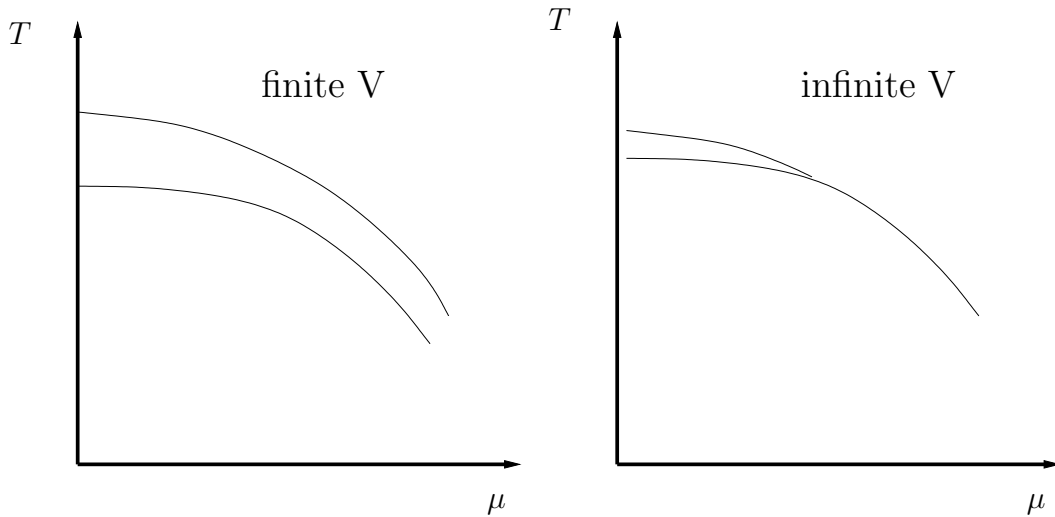


Figure 2: *Schematic location of the lines defined by Eq. (11). In the infinite volume limit (right), the lines merge for a phase transition, but stay separate for a crossover, the bifurcation marking the end point of the phase transition.*

to infinity, the mountain ridge changes its shape: where there is a phase transition, it becomes singular and infinitely narrow, i.e. the two lines merge into one. Where there is a crossover, the ridge saturates at finite height with finite curvature, and the two lines remain separate (as in Fig. 2 (right) at small  $\mu$ ). In this case there is no phase transition and no uniquely defined pseudo-critical line. Nevertheless, the physical properties change rapidly in the region of the line defined by  $\partial_{\beta}\chi = 0$ , as is

well known from the zero density case. Moreover, for small  $\bar{\mu}$  this line is the one closer to the ridge. Thus, for every  $\bar{\mu}$  we may locate the thermal transition by the conditions specified in Eq. (10), which then represent our implicit definition of the critical line  $\beta_c(\bar{\mu})$ .

Let us now consider a finite volume. Expanding the susceptibility around  $\beta_c(0)$  and using  $\chi(\bar{\mu}, \beta) = \chi(-\bar{\mu}, \beta)$ , it takes the form

$$\chi(\bar{\mu}, \beta) = \sum_{n,m=0} c_{nm} (\beta - \beta_c(0))^n \bar{\mu}^{2m}. \quad (12)$$

Because  $\chi(\bar{\mu}, \beta)$  is analytic, its derivatives are as well. In the neighbourhood of the critical line we furthermore have  $\partial_{\beta}^2 \chi \neq 0$ . The implicit function theorem<sup>2</sup> then tells us that the implicitly defined  $\beta_c(\bar{\mu})$  is analytic in  $\bar{\mu}$ . Furthermore, its first derivative is obtained from the chain rule for partial differentiation,

$$\frac{\partial \beta_c}{\partial \bar{\mu}} = - \frac{\partial^2 \chi}{\partial \bar{\mu} \partial \beta} \left( \frac{\partial^2 \chi}{\partial \beta^2} \right)^{-1}. \quad (13)$$

Since  $\chi$  is even in  $\bar{\mu}$ , the same follows from the last equation for  $\beta_c$ , which therefore has a Taylor expansion

$$\beta_c(\bar{\mu}) = \sum_{n=0} a_n \bar{\mu}^{2n} = \sum_{n=0} c_n (a\mu)^{2n}, \quad (14)$$

where we have absorbed the temporal lattice length into the coefficients in the second equation,  $c_n = a_n N_t^{2n}$ .

All of these considerations are unchanged if we consider a purely imaginary potential,  $\bar{\mu} = i\bar{\mu}_I$ . In this case we may define a corresponding real function  $\tilde{\chi}(\bar{\mu}_I, \beta)$  with a Taylor expansion in  $\beta, \bar{\mu}_I^2$  and coefficients  $\tilde{c}_{nm}$ . Clearly, this is just the analytic continuation  $\tilde{\chi}(\bar{\mu}_I, \beta) = \chi(i\bar{\mu}_I, \beta)$ , with  $\tilde{c}_{nm} = c_{nm}(-1)^m$ . Its maximum in the  $\beta$ -direction is again defining a function  $\beta_c(\bar{\mu}_I)$ , which by the implicit function theorem is analytic. The analogue of Eq. (13) then reads

$$\frac{\partial \beta_c}{\partial \bar{\mu}_I} = - \frac{\partial^2 \tilde{\chi}}{\partial \bar{\mu}_I \partial \beta} \left( \frac{\partial^2 \tilde{\chi}}{\partial \beta^2} \right)^{-1} = -i \frac{\partial^2 \chi}{\partial \bar{\mu} \partial \beta} \left( \frac{\partial^2 \chi}{\partial \beta^2} \right)^{-1} = i \frac{\partial \beta_c}{\partial \bar{\mu}}. \quad (15)$$

Since this equation is true for every  $\bar{\mu}_I < \bar{\mu}_I^c$  we have thus established  $\beta_c(\bar{\mu}_I) = \beta_c(\bar{\mu} = i\bar{\mu}_I)$ , i.e. the critical line of the deconfinement transition at imaginary chemical potential is simply the analytic continuation of the critical line at real chemical potential.

---

<sup>2</sup>See e.g. [20]. We thank F. Wilczek for reminding us of this theorem in this context.



Next, we need to discuss the infinite volume limit. As remarked above, for every  $\bar{\mu}$  the critical coupling will approach its thermodynamic limit in a fashion characteristic of the order of the transition. However,  $\beta_c(\infty, \bar{\mu})$  is only shifted from  $\beta_c(V, \bar{\mu})$ , without developing any singularities in the thermodynamic limit. Hence, the critical line defined by Eq. (10) marks the singularities in the partition function, which it smoothly connects to a pseudo-critical line in the crossover region. It thus remains itself an analytic function of  $\bar{\mu}$  in the thermodynamic limit for all  $\bar{\mu}$ .

Our strategy is now to first compute the critical line for imaginary chemical potential and check the convergence of its Taylor expansion. As we shall see, convergence is surprisingly fast for the whole range of chemical potentials accessible to this method. Analytic continuation then reduces to simply flipping the sign of the appropriate terms. Finally, the infinite volume limit has to be taken from the continued results at real  $\bar{\mu}$ . The order of the transition can then be determined in a  $(V, \bar{\mu})$ -range where the truncation error of the series is smaller than finite size scaling effects.

## 4 Numerical results for two light flavors

In order to test the feasibility of our approach, we consider QCD with two flavors of staggered fermions with bare mass  $am = 0.025$  and  $\mu_R = 0$  on a  $8^3 \times 4$  lattice. We use the R-algorithm [21] with a step size  $\delta\tau = 0.02$ , sufficiently small for the systematic errors  $\mathcal{O}(\delta\tau^2)$  to be negligible compared to our statistical errors. For 8 values of  $\beta$  spanning the relevant temperature regime and 6 values of  $a\mu_I \in \{0, \pi/12\}$ , we have accumulated 2000 – 6000 unit-length trajectories each, measuring the gauge action, the Polyakov loop and the chiral condensate after each trajectory. For one parameter set we have performed additional simulations on  $6^3 \times 4$ . To determine the pseudo-critical value  $\beta_c(a\mu_I)$ , we use the Ferrenberg-Swendsen reweighting method [22].

### 4.1 The Z(3) transition for imaginary $\mu$

First, it is instructive to investigate the Z(3) transition discussed in Sec. 2. The predicted critical value for the chemical potential is at  $\bar{\mu}_I^c = \pi/3$ , which on our  $N_t = 4$  lattice corresponds to  $a\mu_I^c = \pi/12 = 0.262$ . For this value Fig. 3 shows histograms of the phase  $\varphi$  of the Wilson loop, obtained for various lattice couplings (temperatures). We find the system tunneling between the sectors with  $\varphi = 0$  and  $\varphi = -2\pi/3$ .

In accord with the predictions made in [13], we observe a smooth distribution consistent with a crossover at low temperatures, and a pronounced two-state signal indicating a first order phase transition at high temperatures. The critical coupling for the onset

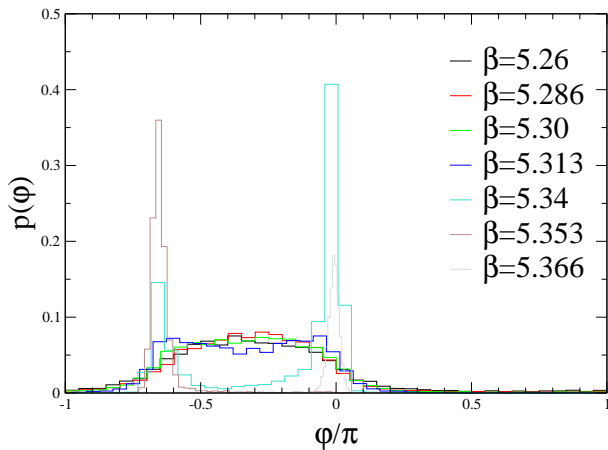


Figure 3: *Probability distribution of the phase of the Polyakov loop for the critical value  $a\mu_I^c = \pi/12$ .*

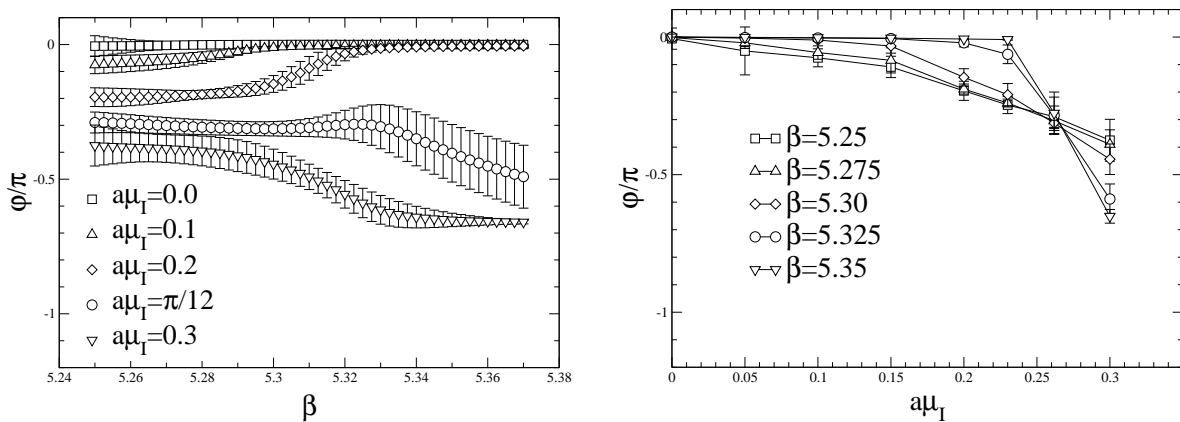


Figure 4: *The  $\beta$ - and  $\mu_I$ -dependence of the average phase of the Polyakov loop.*

of the  $Z(3)$  transition is visibly between  $5.313 < \beta_c < 5.34$ .

For low temperatures, where the  $Z(3)$  transition is continuous, there is frequent tunneling between the  $Z(3)$  sectors. It then follows that also for  $a\mu_I < (a\mu_I)^c$  the ensemble average consists of a mixture of the two sectors, where the  $\varphi = -2\pi/3$  admixture grows with  $a\mu_I$ . This is clearly visible in Fig. 4, where the average phase of the Polyakov loop gradually moves from  $\varphi(a\mu_I = 0) = 0$  to  $\varphi((a\mu_I)^c) = -\pi/3$ , the latter value corresponding to the average between the two phases  $\varphi = 0, -2\pi/3$ . For

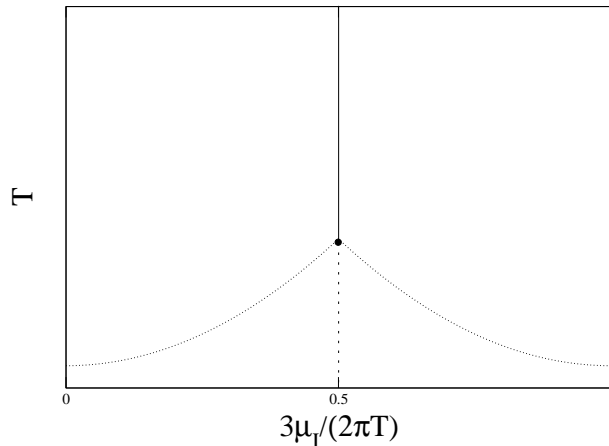


Figure 5: *Schematic phase diagram for imaginary chemical potential: The vertical line marks the  $Z(3)$  transition (this section), the curved lines the deconfinement transition (next section). The solid line indicates a first order transition, while the nature of the dotted lines is not yet determined. The diagram is periodically repeated for larger values of  $\mu_I$ .*

$a\mu_I > (a\mu_I)^c$ , the phase gets dominated by the vacuum with  $\varphi = -2\pi/3$ .

At high temperatures, on the other hand, the  $Z(3)$  sectors are separated by a diverging potential barrier, and tunneling is more suppressed the higher the temperature. As a result the Monte Carlo ensemble stays longer in one sector, and its equilibrium is dominated by the lowest vacuum. Thus, as shown in Fig. 4, for  $a\mu_I < (a\mu_I)^c$  the system always settles in the trivial vacuum with zero phase, whereas for  $a\mu_I > (a\mu_I)^c$  it settles in the vacuum sector with  $\varphi = -2\pi/3$ . The dividing line between those situations is  $\varphi((a\mu_I)^c) = -\pi/3$ , which is independent of temperature by symmetry. In Fig. 4, one observes that indeed  $\varphi((a\mu_I)^c) = -\pi/3$  for all  $\beta$ 's, although errors become large at large  $\beta$ . This reflects the difficulty of tunneling at high temperatures, and implies longer and longer Monte Carlo time for the system to equilibrate. Hence, at high temperatures great attention must be paid to  $Z(3)$  ergodicity and its possible violation.

From the susceptibilities  $\chi(\beta)$  at  $(a\mu_I)^c = \pi/12$ , only one peak is apparent. This means that, within our accuracy, at  $(a\mu_I)^c$  the critical temperature at which the  $Z(3)$  first-order transition line starts is the same as the critical temperature for the deconfinement transition determined below. Schematically the  $(T, \mu_I)$  phase diagram then looks as in Fig. 5, with a special point where three critical lines meet. This point might

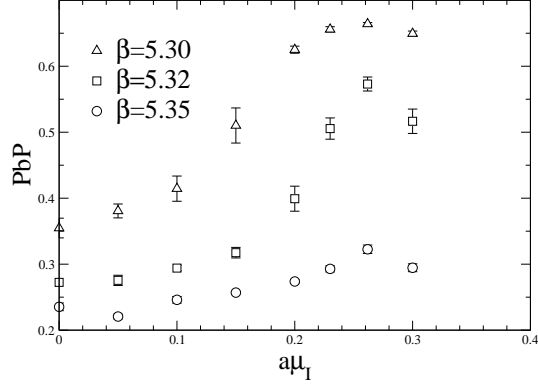


Figure 6: *The chiral condensate  $\bar{\psi}\psi$  as a function of  $a\mu_I$ .*

be tricritical if deconfinement corresponds to a genuine phase transition, or critical otherwise. We take a first look at this issue below.

Once ergodicity is ensured, the effects of the  $Z(3)$  transition are also visible in other observables like, e.g., the chiral condensate, as shown in Fig. 6. Note the symmetry of the observable around  $a\mu_I^c$  according to Eq. (7). For low  $\beta$  (viz. temperatures) the observable is continuous at the critical chemical potential, while a cusp indicating a discontinuous transition develops for large  $\beta$ .

Let us now try to determine the endpoint ( $\beta_c, a\mu_I = \pi/12$ ) of the first-order transition

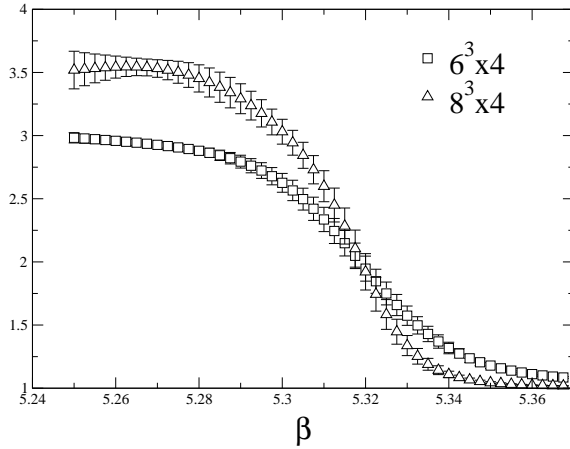


Figure 7: *Ratio of of cumulants  $\langle \hat{\varphi}^4 \rangle / \langle \hat{\varphi}^2 \rangle^2$ , for  $a\mu_I = \pi/12$ .*

line with better accuracy. We can do so by monitoring the plaquette susceptibility as a function of  $\beta$ . This procedure gives us  $\beta_c = 5.325(5)$ . For improved accuracy, and to check our control of the delicate ergodicity problems mentioned above, we performed additional simulations on a  $6^3 \times 4$  lattice at  $a\mu_I = \pi/12$ . Since  $\varphi = -\pi/3$ , one can form a ratio of cumulants  $\langle \hat{\varphi}^4 \rangle / \langle \hat{\varphi}^2 \rangle^2$ , where  $\hat{\varphi} = \varphi + \frac{\pi}{3}$ , and estimate the critical point  $\beta_c$  from the crossing of the cumulant ratios for the two available volumes. This procedure, illustrated in Fig. 7, yields a consistent value  $\beta_c = 5.321(7)$ . Note also that the crossing occurs at a value of the cumulant ratio 1.8(2) consistent with that of the  $3d$  Ising universality class 1.604(1) [23]. This indicates as the simplest interpretation of the phase diagram: the first-order  $Z(3)$  transition line ends with a second-order critical point in the Ising class. This picture will likely depend on the number of quark flavors and on their masses.

## 4.2 The deconfinement transition for imaginary $\mu$

In order to map out the deconfinement transition line in the  $(\beta, \bar{\mu}_I)$ -plane, we have measured the susceptibility of the plaquette, of the modulus of the Polyakov loop, and the disconnected part of a stochastic estimator for the chiral condensate susceptibility. All three observables yield consistent results for  $\beta_c(a\mu_I)$ , as shown in Fig. 8. We have chosen to display only three  $a\mu_I$ -values for clarity of the plots. Note that the critical lattice coupling is growing with increasing  $a\mu_I$ , and thus the critical temperature is an increasing function of  $\mu_I$  as well. This is in contrast to the situation at real  $\mu$ , where  $T_c(\mu)$  is a decreasing function. This qualitative behaviour is in accord with the one found for screening lengths in units of inverse temperature, which are increasing

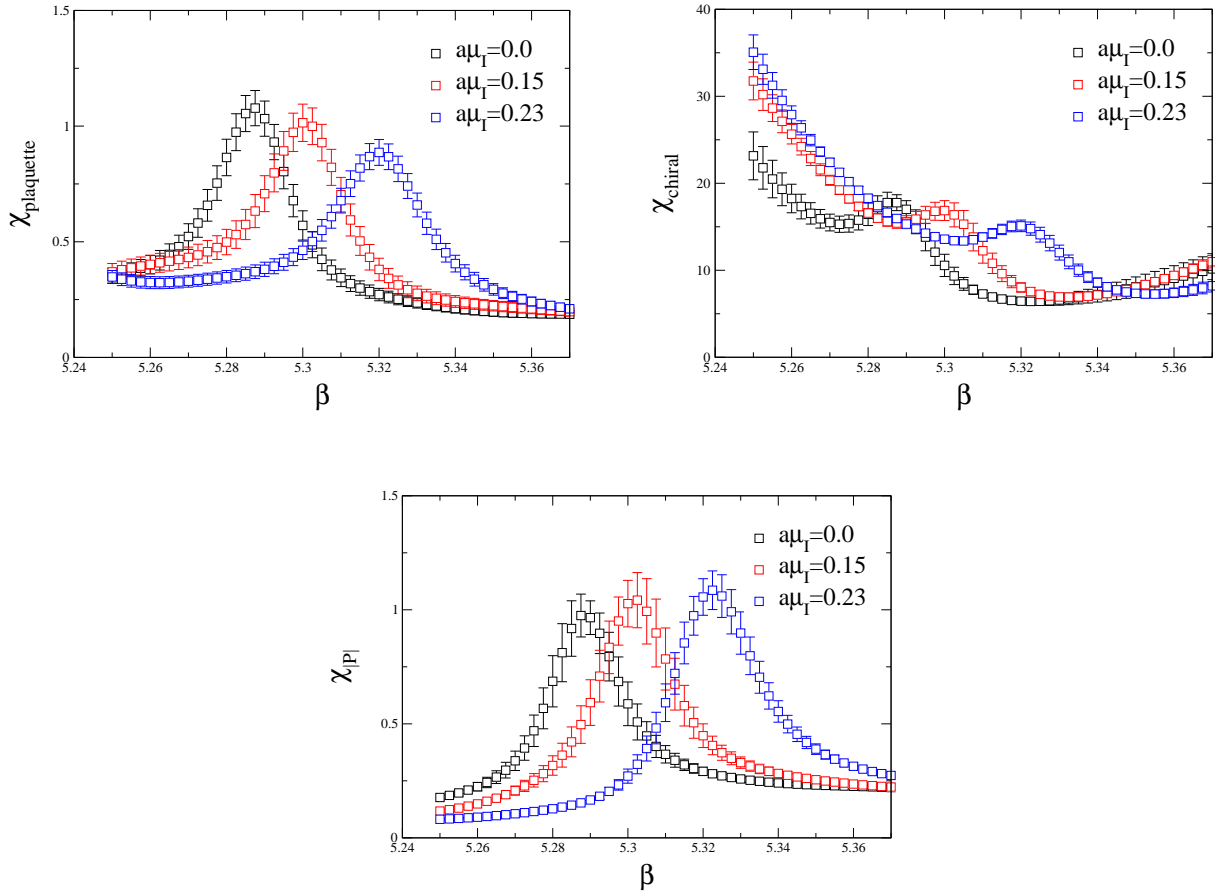


Figure 8: *Susceptibilities for the plaquette, the chiral condensate and the absolute value of the Polyakov loop.*

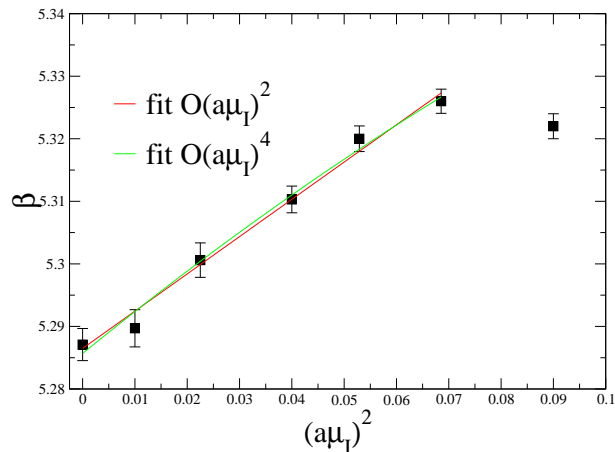


Figure 9: Location of the pseudo-critical deconfinement line as determined from plaquette susceptibilities. The lines show the fits given in Table 1.

| $\beta_c$ from $\chi_{plaq}$ | $c_0$      | $c_1$     | $c_2$      | $\chi^2/\text{dof}$ | $Q$  |
|------------------------------|------------|-----------|------------|---------------------|------|
| $\mathcal{O}((a\mu_I^2))$    | 5.2865(18) | 0.596(40) | –          | 0.60                | 0.66 |
| $\mathcal{O}((a\mu_I^4))$    | 5.2857(23) | 0.68(15)  | –1.2 (2.0) | 0.67                | 0.57 |
| $\beta_c$ from $\chi_{ P }$  | $c_0$      | $c_1$     | $c_2$      | $\chi^2/\text{dof}$ | $Q$  |
| $\mathcal{O}((a\mu_I^2))$    | 5.2874(17) | 0.640(38) | –          | 0.29                | 0.89 |
| $\mathcal{O}((a\mu_I^4))$    | 5.2873(21) | 0.65(14)  | –0.2 (2.0) | 0.38                | 0.77 |

Table 1: The first coefficients of the Taylor expansion of the critical coupling, Eq. (14). Data and fits for  $\beta_c$  from  $\chi_{plaq}$  are shown in Fig. 9.

(decreasing) functions of  $\mu_I$  ( $\mu_R$ ) [8]. (An increasing screening length means more energy is required to separate charges before they are screened, and hence an increasing deconfinement temperature).

Since the plaquette susceptibility is the one that is most accurately determined, it is our choice for determining the critical line. The values of  $\beta_c$  corresponding to six values of  $a\mu_I$  are shown in Fig. 9. Our next task is to determine the reliability of the Taylor expansion for the critical line, Eq. (14). Results of fitting the data to a polynomial of degree one and two in  $(a\mu_I)^2$ , respectively, are shown in Table 1 and Fig. 9. Excellent fits are obtained in both cases with compatible coefficients  $c_{0,1}$ . The quartic correction appears negligible even near  $a\mu_I = (a\mu_I)^c$ , leaving  $c_2$  to be

consistent with zero within this range. This is again in accord with the analogous finding for screening masses, which are equally well described by the leading  $(a\mu_I)^2$  term in that range [8]. Statistically consistent results are obtained when  $\beta_c$  is extracted from Polyakov loop instead of plaquette susceptibilities, as also shown in Table 1. We then conclude that the (pseudo-) critical line for imaginary chemical potential  $\bar{\mu} = i\bar{\mu}_I$ ,  $\bar{\mu}_I \leq \pi/3$ , is well described by

$$\beta_c(a\mu_I) = c_0 + c_1(a\mu_I)^2, \quad (16)$$

with  $c_0, c_1$  as per Table 1 (top line).

### 4.3 The deconfinement transition in physical units for real $\mu$

With the results of the previous section, it is now trivial to obtain  $\beta_c(\bar{\mu})$  for real  $\bar{\mu}$ , by continuing  $\bar{\mu}_I \rightarrow -i\bar{\mu}_I$ . As a comment on systematics, let us add that the difference between the linear and quadratic fits in  $(a\mu_I)^2$  from Table 1 gets slightly amplified by analytic continuation (only the sign of one term is flipped). This reflects the fact that convergence properties in the real and imaginary directions may be different in general. Such an effect will be large for an observable with pronounced structures, and small on a smooth observable like ours. In any case, the effect can be monitored, and the error band of the first fit is even after continuation completely contained within the error band of the second fit, which can hence be dropped as statistically insignificant.

It is instructive to translate our result into physical units, in order to illustrate the phenomenological relevance of our approach. However, we caution that at this stage such a conversion is merely illustrative, with quantitative numbers still afflicted by various systematic errors: while we have monitored that the truncation error of the Taylor series is negligible, there might still be sizeable corrections from finite volume and lattice spacing effects, and we have not investigated the quark mass dependence of our results. In view of this we content ourselves with the perturbative two-loop expression for the lattice QCD scale  $\Lambda_L$  in the presence of two massless flavors,

$$\begin{aligned} a(\beta)\Lambda_L &= \left(\frac{6b_0}{\beta}\right)^{-b_1/2b_0^2} \exp(-\beta/12b_0), \\ b_0 &= \frac{1}{16\pi^2} \left(11 - \frac{2}{3}N_f\right), \quad b_1 = \left(\frac{1}{16\pi^2}\right)^2 \left(102 - \frac{38}{3}N_f\right), \\ \frac{T_c(\mu)}{T_c(0)} &= \frac{a(\beta_c(\mu))\Lambda_L}{a(\beta_c(0))\Lambda_L} \end{aligned} \quad (17)$$

while the scale is set by the critical temperature  $T_c(\mu = 0) = 173(8)\text{MeV}$  in the chiral limit for staggered fermions [24] (which is expected to still contain finite lattice spacing



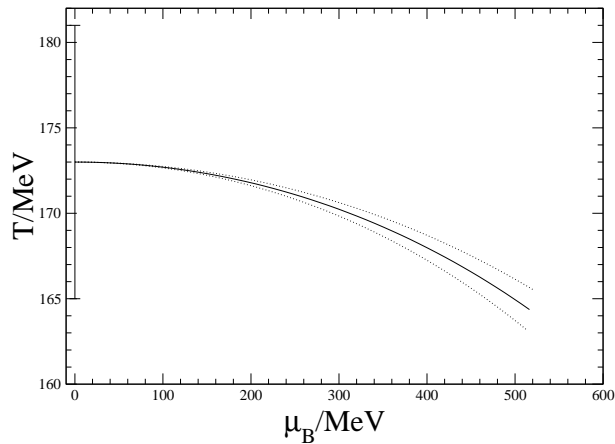


Figure 10: *Location of the deconfinement transition corresponding to the first fit in Table 1. The error bar gives the uncertainty in  $T_c(0)$  used to set the scale, the dotted lines reflect the error on  $c_1$  from Table 1.*

errors). This leads to the result for the (pseudo-) critical line as shown in Fig. 10. As remarked before, a detailed finite volume study is beyond the scope of the present work but would reveal the order of the transition along the line.

## 5 Comparison with other methods

Before concluding, we would like to make some comments comparing our method with previous studies of the finite  $\mu$  deconfinement transition [2, 5]. The main disadvantage of our approach is its limitation to the range  $|\mu|/T < \pi/3$ , as discussed in Sec. 2. On the other hand, within this range we have full control over the necessary approximation, i.e. the truncation of the Taylor series, which we find to pose no limitation at all within the accessible range.

We would like to illustrate the importance of this aspect by a comparison with the reweighting method [3, 2]. In Ref. [3], the overlap of the reweighted with the full ensemble is tested for imaginary  $\mu$ . The configurations used for reweighting from the  $\mu = 0$  ensemble are all in the real  $Z(3)$  sector, so that reweighting is by construction insensitive to the  $Z(3)$  transition. This is clearly seen in Fig. 1 of Ref. [3], where the reweighted chiral condensate is found to be a monotonically increasing function of  $(a\mu_I)$  in the range  $0 \leq a\mu_I \leq 0.32$ . Such a result is inconsistent with the symmetries of the imaginary- $\mu$  theory. Ref. [3] works at the same lattice spacing as we do, and therefore

the critical chemical potential for  $Z(3)$  tunneling is at  $(a\mu_I)^c = \pi/12$ . According to Eq. (7), the chiral condensate has to be symmetric about this point and decrease for larger  $a\mu_I$ , as it does in our data, Fig. 6. Not surprisingly, reweighting completely misses this qualitative behavior<sup>3</sup>. In the case of real  $\mu$ , there is no  $Z(3)$  transition. However, the relevance of complex  $Z(3)$  sectors was studied in [17]. It was argued there that constraining the Polyakov loop to be real is a reasonable approximation below and above the deconfinement transition, but a poor one near it. In any case, the discussion illustrates a potential danger of any reweighting method: it may completely miss a qualitative change in the physics without announcing its failure, which only shows up by comparison with results obtained without reweighting.

Ref. [2] studied  $N_f = 2 + 1$  flavors, with light quark mass values and lattice spacing as ours, whereas the bare strange quark mass was chosen eight times heavier than the light ones. Keeping this difference in mind, we find the location of our continuum transition line consistent with theirs over the whole range we have studied.

As mentioned in the introduction, another recent work [5] employs a Taylor expansion of the reweighted path integral. However, in this case only susceptibilities are measured, so that one has no control over the higher order terms. Let us recall that the Taylor expansion is in  $\mu/T$ , which becomes larger than one already at  $\mu \sim 170$  MeV. A priori there is no way of knowing how large the convergence radius of such an expansion is. Simulating at imaginary  $\mu$  provides a framework for obtaining quantitative information about the convergence. As it turns out, our results non-perturbatively endorse the use of the leading Taylor coefficient in  $T_c(\mu)$  up to  $\mu \sim 170$  MeV. Ref. [5] works at quark masses four to ten times larger than ours, but finds only very weak quark mass dependence. Keeping this difference in mind, we find our result for the slope  $c_1$  of  $\beta_c((a\mu)^2)$  to be consistent with theirs.

## 6 Conclusions

The past year has seen progress in the numerical study of finite density QCD. However, this progress is essentially based on adopting a more pragmatic viewpoint. The net quark density in heavy-ion collisions is small. Therefore, instead of solving the fundamental difficulty posed by the sign problem, it is very useful already to explore the regime of small chemical potential, where the sign problem is moderate and various

---

<sup>3</sup>Fig. 1 of Ref. [3] also shows the chiral condensate rising monotonically in the *full* ensemble. A possible reason for this strange behavior might be insufficient thermalization, cf. the discussion in Sec. 4.1. Indeed, at yet larger  $\mu_I$ , the authors of Ref. [3] find, as expected, clear disagreement between reweighted and full ensemble results [25].

approaches appear possible.

We have studied QCD with two light flavors of staggered fermions in the presence of an imaginary chemical potential  $\mu = i\mu_I$ . In this case the partition function is periodic in  $\mu_I$  and, in addition to the deconfinement transition,  $Z(3)$  transitions occur at  $(\mu_I/T)_c = 2\pi(n+1/2)/3$ . We mapped out the phase diagram in the  $(T, \mu_I)$ -plane and found that the  $Z(3)$  transitions are of first order in the deconfined phase and continuous in the confined phase. For  $(\mu_I/T) < \pi/3$ , the critical temperature for deconfinement is an analytic function, irrespective of the order of the transition. Within this range its Taylor expansion is found to rapidly converge and to be well described by the leading term.

Other recent work uses reweighting of simulations performed at  $\mu = 0$ , and at one or more temperatures. In contrast, we vary two parameters in our simulations: the temperature as usual, and also the imaginary chemical potential  $\mu_I$ . Having at our disposal two-dimensional information allows us a reasonable control over systematic errors.

We have used this property to determine the transition line  $T_c(\mu)$  for real  $\mu$  through analytic continuation. While we cannot, on a single volume, find out whether the transition is a crossover or a genuine phase transition at each value of  $\mu$ , a finite-size scaling study should elucidate this issue, provided that finite size effects are larger than the truncation error. Our central result is shown in Fig. 10. It is consistent with Refs. [2, 5]. The transition line is well represented by the equation

$$\frac{T_c(\mu_B)}{T_c(\mu_B = 0)} = 1 - 0.00563(38) \left(\frac{\mu_B}{T}\right)^2, \quad (18)$$

while the next-order term  $\mathcal{O}((\mu_B/T)^4)$  is statistically insignificant up to  $\mu_B \sim 500$  MeV.

**Acknowledgements:** We thank V. Azcoiti, O. Bär, Z. Fodor, M. García Pérez, M. Laine, M.-P. Lombardo, K. Rajagopal and F. Wilczek for discussions and comments.

## References

- [1] S. Hands, Nucl. Phys. Proc. Suppl. **106** (2002) 142 [arXiv:hep-lat/0109034]; O. Philipsen, Nucl. Phys. Proc. Suppl. **94** (2001) 49 [arXiv:hep-lat/0011019]; arXiv:hep-ph/0110051.
- [2] Z. Fodor and S. D. Katz, JHEP **0203** (2002) 014 [arXiv:hep-lat/0106002].
- [3] Z. Fodor and S. D. Katz, arXiv:hep-lat/0104001;
- [4] I. M. Barbour, S. E. Morrison, E. G. Klepfish, J. B. Kogut and M. P. Lombardo, Nucl. Phys. Proc. Suppl. **60A** (1998) 220 [arXiv:hep-lat/9705042].
- [5] C. R. Allton *et al.*, arXiv:hep-lat/0204010.
- [6] S. Gottlieb *et al.*, Phys. Rev. D **38** (1988) 2888; P. de Forcrand *et al.* [QCD-TARO Collaboration], hep-lat/0011013; S. Choe *et al.*, Phys. Rev. D **65**, 054501 (2002); R. V. Gavai, S. Gupta and P. Majumdar, Phys. Rev. D **65** (2002) 054506 [arXiv:hep-lat/0110032].
- [7] M. P. Lombardo, Nucl. Phys. Proc. Suppl. **83** (2000) 375 [arXiv:hep-lat/9908006].
- [8] A. Hart, M. Laine and O. Philipsen, Phys. Lett. B **505** (2001) 141 [arXiv:hep-lat/0010008].
- [9] A. Hart, M. Laine and O. Philipsen, Nucl. Phys. B **586** (2000) 443 [arXiv:hep-ph/0004060].
- [10] P. Ginsparg, Nucl. Phys. **B170** (1980) 388; T. Appelquist and R. D. Pisarski, Phys. Rev. **D23** (1981) 2305.
- [11] K. Rajagopal, Nucl. Phys. A **661** (1999) 150 [arXiv:hep-ph/9908360].
- [12] J. Cleymans and K. Redlich, Phys. Rev. C **60** (1999) 054908 [nucl-th/9903063]; and references therein.
- [13] A. Roberge and N. Weiss, Nucl. Phys. B **275** (1986) 734.
- [14] D. J. Gross, R. D. Pisarski and L. G. Yaffe, Rev. Mod. Phys. **53** (1981) 43; N. Weiss, Phys. Rev. D **24** (1981) 475.
- [15] V. Dixit and M. C. Ogilvie, Phys. Lett. B **269** (1991) 353; J. Ignatius, K. Kajantie and K. Rummukainen, Phys. Rev. Lett. **68** (1992) 737.

- [16] C. P. Korthals Altes, R. D. Pisarski and A. Sinkovics, Phys. Rev. D **61** (2000) 056007 [arXiv:hep-ph/9904305].
- [17] P. de Forcrand and V. Laliena, Phys. Rev. D **61**, 034502 (2000) [arXiv:hep-lat/9907004].
- [18] M.N. Barber, in *Phase Transitions and Critical Phenomena*, eds. C. Domb and J.L. Lebowitz (Academic Press, New York, 1983), Vol 8.
- [19] M. Fukugita, M. Okawa and A. Ukawa, Nucl. Phys. B **337** (1990) 181; Y. Iwasaki *et al.*, Phys. Rev. D **46** (1992) 4657.
- [20] See, e.g., P. Henrici, "*Applied and computational complex analysis*", 1974, Wiley Pub., Th. 2.4d, p.101.
- [21] S. Gottlieb, W. Liu, D. Toussaint, R. L. Renken and R. L. Sugar, Phys. Rev. D **35**, 2531 (1987).
- [22] A. M. Ferrenberg and R. H. Swendsen, Phys. Rev. Lett. **63**, 1195 (1989).
- [23] H.W.J. Blöte, E. Luijten and J.R. Heringa, J. Phys. A: Math. Gen. 28 (1995) 6289 [arXiv:cond-mat/9509016]
- [24] F. Karsch, E. Laermann and A. Peikert, Nucl. Phys. B **605** (2001) 579 [arXiv:hep-lat/0012023].
- [25] Z. Fodor, private communication.